ISSN 0023-1584, Kinetics and Catalysis, 2008, Vol. 49, No. 6, pp. 791–801. © Pleiades Publishing, Ltd., 2008.
Original Russian Text © A.S. Ivanova, E.V. Kul'ko, O.V. Klimov, G.A. Bukhtiyarova, G.S. Litvak, A.A. Budneva, E.A. Paukshtis, D.A. Zyuzin, E.M. Moroz, V.I. Zaikovskii, A.S. Noskov, 2008, published in Kinetika i Kataliz, 2008, Vol. 49, No. 6, pp. 833–843.

Influence of the Texture and Acid–Base Properties of the Alumina-Containing Support on the Formation of Co(Ni)–Mo Catalysts for Deep Hydrodesulfurization of the Diesel Fraction

A. S. Ivanova, E. V. Kul'ko, O. V. Klimov, G. A. Bukhtiyarova, G. S. Litvak, A. A. Budneva, E. A. Paukshtis, D. A. Zyuzin, E. M. Moroz, V. I. Zaikovskii, and A. S. Noskov

Boreskov Institute of Catalysis, Siberian Branch, Russian Academy of Sciences, Novosibirsk, 630090 Russia
e-mail: iva@catalysis.nsk.su

Received February 27, 2008

Abstract—The influence of the texture of γ-Al_2O_3 on the formation of Co(Ni)–Mo catalysts for hydrodesulfurization of the diesel fraction is studied. As shown by low-temperature N_2 adsorption, X-ray diffraction, IR spectroscopy of adsorbed molecules, and high resolution electron microscopy (HREM), use of a support with a larger specific surface and a lower total concentration of terminal OH groups makes it possible to prepare more active catalysts. The electron density radial distribution method shows that the finely dispersed cobalt-containing catalyst in its initial state contains $CoMoO_4$, $Al_2(MoO_4)_3$, and $CoAl_2O_4$, the last two phases being present in trace amounts. After the reaction, this catalyst contains cobalt-doped molybdenum sulfide. According to HREM data, the active phase of the cobalt-containing catalyst consists of layered sulfide association species $Co_{1.3}Mo_2S_{3.3}$, which differ in composition from the bulk phase $CoMo_2S_4$. It is assumed that, out of the 1.3 cobalt atoms in $Co_{1.3}Mo_2S_{3.3}$ 0.3 Co occurs at the edges of the association species and 1.0 Co is intercalated into their interlayer space, and 0.7 S at the boundary between the association species and the Al_2O_3 phase is replaced by the corresponding amount of oxygen.

DOI: 10.1134/S0023158408060049

INTRODUCTION

A new motor fuel specification has been developed to comply with the increasingly stringent regulations being imposed on the concentrations of noxious compounds in automotive exhaust. In particular, in Europe sulfur in diesel fuel must be reduced to 10 ppm by 2010 [1–3]. In straight-run diesel distillates obtained from oils of various origins, the ratio between thiophene derivatives and other sulfur-containing compounds, which are thermodynamically less stable to hydrogenolysis, can vary significantly (from 1 : 4 to 3 : 2) [1]. In feedstocks containing up to 30% catalytic cracking, viscosity breaking, and coking products, the fraction of thiophene derivatives is larger and they account for more than 50% of the total amount of sulfur. The problem of deep hydrodesulfurization is complicated by the steady increase in both the total sulfur content of crude oil and in the contribution from the thiophene derivatives to the total sulfur content [2]. Therefore, it is necessary to create new, more active catalysts for the deep hydrodesulfurization of diesel fuel.

Co(Ni)–Mo/Al_2O_3 catalytic systems are most frequently used for this purpose in industry. It was shown [4–10] that the catalytic activity in hydrodesulfurization is determined by the Co–Mo–S phase, which consists of fine MoS_2 particles, whose edges contain Co(Ni). A detailed analysis of the *K*-edge EXAFS spectra shows that there are two types of Co–Mo–S phases with different structural properties [11]. The phase exhibiting high hydrodesulfurization activity has six Co–S coordination bonds and two Co–Mo coordination bonds. The other phase, with a lower activity, has five Co–S coordination bonds and one Co–Mo bond. The nature of the support (in particular, the promotion of Al_2O_3 by B, F, P, and other anions) affects the formation of the active phase by modifying its local structure [4, 5, 12, 13]. In addition, the support usually exerts an effect on the distribution of the active component and on its degree of dispersion. Thus, the surface properties and texture of the support can be the key factors in the formation of an active catalyst.

The purpose of this work is to study the influence of the texture and acid–base properties of the alumina-containing support on the structural, textural, acid–base, and catalytic properties of Co(Ni)–Mo catalysts for deep hydrodesulfurization of the diesel fraction.

EXPERIMENTAL

The catalyst precursors Co(Ni)–Mo–O/Al_2O_3 were prepared by the incipient-wetness impregnation of the support with salt solutions [14]. The support was

γ-Al_2O_3 obtained by thermal treatment of pseudoboehmite synthesized either via the hydration of the product of the centrifugal thermal activation of hydrargillite (CTA product) [15] or via precipitation. The impregnating solutions were prepared using ammonium molybdate ($(NH_4)_6Mo_7O_{24} \cdot 4H_2O$), nickel or cobalt nitrate ($Ni(NO_3)_2 \cdot 4H_2O$ or $Co(NO_3)_2 \cdot 4H_2O$), phosphoric and citric acids, and a poly(ethylene oxide) solution. The catalysts were dried in an oven at 110–120°C for 12–14 h and were then calcined at 500–550°C for 4 h.

The main components in the resulting catalysts were quantified by atomic absorption spectrometry [16]. Thermal analyses were carried out on a Q 1500-D thermoanalytical system in the temperature range from 20 to 1200°C at a heating rate of 10 K/min in air. The sample weight was 0.2 g, and the accuracy of weight loss determination was ±0.5%.

X-ray diffraction analyses were carried out on an HZG-4C diffractometer using monochromated CuK_α radiation (λ = 1.5418 Å). The coherent-scattering domain size (D) was calculated using the Selyakov–Scherrer formula [17]. The accuracy of the determination of the unit cell parameter a of alumina was ±0.005 Å. A number of samples were characterized by X-ray diffraction at the Synchrotron Radiation Station of the Siberian Center (Institute of Nuclear Physics, Siberian Branch, Russian Academy of Sciences) using a high-resolution diffractometer. A Si(111) monochromator crystal was mounted in the path of the diffraction beam, which made it possible to select radiation with λ = 0.6987 Å and provided a degree of monochromation of $\Delta\lambda/\lambda \approx 10^{-4}$. Scanning was done in the 2θ range from 3° to 135° with 0.1° increments and a counting time of 10 s per point. Electron density radial distribution (EDRD) curves were calculated using a standard procedure [18]. The phase analysis of the crystalline phases was carried out using PC-PDF (JCPDS-ICDD) and ICSD data files. Diffraction patterns for hypothetically known phases were calculated using the PCW program. Intensity difference curves (IDCs) were obtained by subtracting the diffraction pattern of the support from that of the catalyst. The diffraction patterns were preconverted to electron units, taking into account the chemical composition of the samples and incoherent Compton scattering. In order to determine the phase composition of finely dispersed phases by the EDRD method, we constructed model EDRD curves from interatomic distances and structural parameters of known phases, using an earlier reported procedure [19].

Electron micrographs were obtained on a JEM-100C transmission electron microscope (resolution of 30 nm, accelerating voltage of 100 kV).

The specific surface area of catalysts was determined by the thermal desorption of argon [20] with an error of ±10%. Texture parameters were derived from low-temperature (–196°C) nitrogen adsorption isotherms, which were obtained using an ASAP-2400 instrument (Micromeritics).

The acid–base properties of aluminum oxides were studied by IR spectroscopy of adsorbed CO molecules forming complexes with Lewis and Brønsted acid sites [21]. A Shimadzu 8300 FTIR spectrometer with a resolution of 4 cm^{-1} and a spectral accumulation number of 50 was used for this purpose. The samples, compacted without a binder into pellets with a density of $(8–20) \times 10^{-3}$ g/cm^2, were pumped directly into the IR cell for 2 h at 500°C under a pressure below 10^{-4} Torr. CO adsorption was carried out at the liquid nitrogen temperature (–196°C) in the pressure interval from 0.1 to 10 Torr. IR spectra were recorded in the 1200–4000 cm^{-1} range. The lower detection limit for Lewis acid sites (LAS) was 0.2 μmol/g, and the accuracy of quantitative measurements was ±25%.

The catalysts were sulfided and then tested in the hydrodesulfurization of the diesel fraction. The sample to be tested (2 g) was placed into a reactor, and hydrogen sulfide was passed through the reactor at a rate of 1 l/h under reduced pressure, beginning at room temperature and gradually the temperature was raised to 400°C over 30 min. After this temperature was reached, sulfidation was continued for 2 h.

The hydrodesulfurization of the diesel fraction was studied in a flow reactor loaded with a catalyst (2 g, fraction 0.25–0.5 mm). The volumetric feed rate was 2 h^{-1}, the hydrogen pressure was 3.5 MPa, and the H_2/raw material ratio was 300 or 500. The raw material was straight-run diesel fuel with the following characteristics: density at 20°C, 844 kg/m^3; cetane number, 53.5 ± 0.5; congealing point, about –10°C; sulfur content, 1.06% (10600 ppm); flash point (in a close crucible), 66.9°C; fractional makeup: 50 vol % is distillable at 292°C and 96 vol % is distillable at 366°C.

Catalytic activity was estimated as the residual sulfur content of the catalyzate (ppm). The latter was determined with a Horiba SLFA-20 X-ray fluorescence sulfur analyzer.

RESULTS AND DISCUSSION

Properties of the Supports

The structural and textural characteristics of the γ-Al_2O_3 supports examined in this study, which have different unit cell parameters (a), specific surface areas (S_{sp}), pore volumes (V_{por}), and average pore diameters (d_{av}), are presented in Table 1.

The introduction of phosphorus or fluorine into alumina was shown [22–26] to increase the degree of dispersion of the catalytically active phase and the fraction of Brønsted acid sites, which accelerate the migration of methyl groups in particular components of fuels. The character of molybdenum distribution depends on the phosphorus content and on the order in which phosphorus and molybdenum were introduced [27, 28]. If Al_2O_3 is first impregnated with a solution of the phosphorus-containing component, the interaction between them yields amorphous phosphates, which affect the surface

Table 1. Structural and textural characteristics of the supports

Sample Al_2O_3			a, Å	D, Å	S_{sp}, m^2/g	V_{por}, cm^3/g	d_{av}, nm
name	preparation method	calcination temperature, °C					
CTA oxide	From CTA products	600	7.914	55	200	0.29	5.8
Al_2O_3-1	Precipitation	600	7.931	40	285	0.46	6.5
Al_2O_3-2	Precipitation	550	7.922	50	285	0.82	11.5

Table 2. Concentration of OH groups on the surface of various supports

Sample	Concentration of OH groups (in μmol/g) to which absorption bands correspond					ΣC_{OH}, μmol/g
	3680 cm^{-1}	3733/3740 cm^{-1}	3752 cm^{-1}	3775/3770 cm^{-1}	3792 cm^{-1}	
CTA oxide	349	191/38	44	32/18	19	691
Al_2O_3-1	67	73/80	53	36/80	24	413
Al_2O_3-2	130	55	30	30	9	254
P_2O_5/CTA oxide	70	55	30	30	20	205
P_2O_5/Al_2O_3-1	50	30	20	30	20	150

properties of alumina. If the molybdenum-containing component is applied first, it interacts with the support to form a molybdenum- and alumina-containing compound. Subsequent loading of this support or another with cobalt produces Co–Mo–P–O phases with different properties.

IR spectroscopic studies showed (Table 2) that the hydroxyl coating consists of OH groups of two types, namely, terminal and bridging. The three high-frequency absorption bands in Table 2 are assigned to the terminal OH groups, and the two low-frequency bands are assigned to the bridging OH groups.

An analysis of the data in Table 2 shows that the total concentrations of the terminal OH groups (C_{term}, absorption bands at 3792–3752 cm^{-1}) and bridging OH groups (C_{bridg}, 3733–3680 cm^{-1}) decrease in the following orders:

Sample	Al_2O_3-1	CTA oxide	P_2O_5/CTA oxide	P_2O_5/Al_2O_3-1	Al_2O_3-2
C_{term}, μmol/g	193	113	80	70	69
Sample	CTA oxide	Al_2O_3-1	Al_2O_3-2	P_2O_5/CTA oxide	P_2O_5/Al_2O_3-1
C_{bridg}, μmol/g	578	220	185	125	80

Because the bridging OH groups are stronger Brønsted acid sites (BAS) than the terminal groups, the CTA oxide is characterized by the highest surface concentration of BAS and the P_2O_5/Al_2O_3-1 sample has the lowest surface BAS concentration. The introduction of phosphorus into Al_2O_3 decreases the concentration of both terminal and bridging OH groups. Perhaps the decrease in the concentration of hydroxyl groups on the Al_2O_3 surface impedes its interaction with the active components of the catalyst.

An analysis of the IR spectra of adsorbed CO (Table 3) shows that the aluminum oxides considered differ in the total concentration of Lewis acid sites and in the distribution of these sites over their strength. The surfaces of all oxides contain weak LASs corresponding to absorption bands at 2185–2200 cm^{-1}. Medium-strength and strong LASs (absorption bands at 2220 and 2235 cm^{-1}) are also present on the surface of the CTA oxide and Al_2O_3-2. The absorption bands at 2185–2200, 2220, and 2235 cm^{-1} are due to the presence of coordinatively unsaturated surface aluminum cations. The introduction of phosphorus gives rise to an additional absorption band at 2240 cm^{-1}, indicating the formation of strong LASs, whose concentration is higher in the P_2O_5/CTA oxide sample (Table 3). Perhaps the appearance of the strong LASs is due to the formation of $AlPO_4$. Note that the total LAS concentration (ΣC_{LAS}) decreases upon the introduction of phosphorus into CTA oxide, whereas ΣC_{LAS} remains almost unchanged when phosphorus is introduced into Al_2O_3-1.

Table 3. LAS concentration on the surface of various supports

Sample	Concentration (in μmol/g) of LAS to which absorption bands correspond				
	2185–2200 cm^{-1}	2220 cm^{-1}	2235 cm^{-1}	2240 cm^{-1}	ΣC_{LAS}*
CTA oxide	932	19	17	–	968 (4.14)
Al_2O_3-1	695	–	–	–	695 (2.25)
Al_2O_3-2	620	8	1.5	1.5	630 (2.03)
P_2O_5/CTA oxide	660	3.5	1.2	1.8	666 (2.85)
P_2O_5/Al_2O_3-1	685	2.7	0.8	0.3	689 (2.24)

* The numbers in parentheses are ΣC_{LAS} values in μmol/m^2.

Table 4. Chemical composition and catalytic properties of the catalysts

Catalyst*	Support	[Mo]	[Ni] or [Co]	[P]	Ni(Co)/Mo	P/Mo	S_{sp}, m^2/g	Residual content of S**, ppm	
		atom/nm^2						7 h	9 h
Ni-containing catalysts									
NMTs-1	CTA oxide	3.1	0.5	–	0.16	–	210	1136	1132
NMA-2	Al_2O_3-1	2.4	1.1	–	0.45	–	260	1290	1300
NMTs-3-I	P_2O_5/CTA oxide	2.2	1.1	0.31	0.50	0.14	185	312	333
NMA-4-I	P_2O_5/Al_2O_3-1	2.1	1.0	0.26	0.46	0.13	225	175	178
Co-containing catalysts									
KMA-5-I	P_2O_5/Al_2O_3-1	1.9	1.5	0.28	0.79	0.15	200	111	147
KMA-6-IIa	Al_2O_3-2	2.3	1.6	0.19	0.69	0.08	205	54	56
KMA-7-IIa	Al_2O_3-2	2.5	1.5	0.14	0.60	0.06	200	116	118
KMA-8-IIa	Al_2O_3-2	2.4	1.5	0.26	0.63	0.11	220	71	77
KMA-10-IIa	Al_2O_3-2	2.4	1.7	0.22	0.70	0.09	220	25	20
KMA-9-IIb	Al_2O_3-2	2.5	1.5	0.14	0.60	0.06	210	91	99

* I—premodification of the support with phosphorus oxide; IIa—phosphorus oxide is supported simultaneously with the Mo-containing component, and cobalt is supported in the presence of citric acid; IIb—cobalt is supported in the presence of poly(ethylene oxide).

** The activity of the catalysts was estimated by tests under the following conditions: temperature of 350°C, pressure of 35 atm, and H_2/raw materials = 500.

Thus, the introduction of phosphorus into alumina decreases the concentration of hydroxyl groups and affects the LAS distribution over their strength and concentration.

Properties of the Catalysts

The main characteristics of the synthesized Ni(Co)–Mo-containing catalysts are presented in Table 4. The molybdenum content of a catalyst should not exceed the value corresponding to the monolayer coverage [29], because exceeding this level makes possible the formation of MoO_3 or $Al_2(MoO_4)_3$, which reduce the activity of the catalyst. The monolayer coverage is reached when 2.8 Mo atoms occur on 1 nm^2 of the surface [30], and other authors report a value of 3.5–4.0 atoms [31, 32]. However, MoO_3 forms at a molybdenum content of 3.0 atom/nm^2 [29]. As can be seen from the data in Table 4, the molybdenum content of the catalysts does not exceed 2.5 atom/nm^2 (the only exception is the NMTs-1 sample). The Ni/Mo atomic ratio is 0.45–0.50 (with the same exception), and Co/Mo = 0.60–0.79.

The study of the thermolysis stage of the Ni–Mo–$O/P_2O_5/Al_2O_3$ catalysts on the CTA oxide and Al_2O_3-1 supports showed that these samples are similar. The heating of the Mo/Al_2O_3-1 and Mo/CTA oxide samples gives rise to endotherms at 145–151 and 240–244°C (Figs. 1a, 1b). The first of them is due to the removal of physically adsorbed water, and the second endotherm is due to the decomposition of ammonium paramolybdate (Fig. 1c). The exotherms at 430–467°C indicate the completion of the ammonium paramolybdate decomposition stage and the crystallization of molybdenum oxide. The exotherm at 854–880°C (Figs. 1a, 1b) is possibly due to the crystallization of the Mo- and Al-containing compound, and the endotherm at 951–958°C is due to the melting of the Mo-containing compound followed by its vaporization. The exotherm at 1097–1114°C arises from the crystallization of α-Al_2O_3 [33].

The character of the thermolysis of the $Ni(NO_3)_2/Mo/P_2O_5/Al_2O_3$-1 and $Ni(NO_3)_2/Mo/P_2O_5$/CTA oxide samples is also indepen-

Table 5. Textural characteristics of the catalysts and supports derived from low-temperature nitrogen adsorption isotherms

Catalyst	S_{sp}, m^2/g		V_{por}, cm^3/g		d_{av}, nm	
	catalyst	support	catalyst	support	catalyst	support
NMTs-3-I	182	200	0.24	0.29	5.3	5.8
NMA-4-I	220	285	0.41	0.46	6.7	6.5
KMA-10-IIa	220	285	0.49	0.82	10.1	11.5

dent of the type of alumina (Fig. 2). In both cases, the DTA curves show endotherms at 145–159 and 245–259°C due to the removal of physically adsorbed water and nickel nitrate decomposition [34]. The exotherms at 850–857 and 1051–1067°C are possibly due to the crystallization of the Mo–Ni–Al-containing compounds [34], and those at 1131–1135°C arise from the crystallization of α-Al_2O_3. The endotherm at 908–945°C is due to the melting of the Mo-containing compound. Thus, the thermoanalytical data show that the nature of the above alumina-containing supports, which were obtained from different precursors and have different structural and textural properties, exerts no substantial effect on the thermolysis of the supported catalysts.

At the same time, the texture of the catalysts is determined by the texture of the support. It can be seen from the data in Table 4 that the specific surface area of the catalysts based on CTA oxide and P_2O_5/CTA oxide is 185–210 m^2/g and that of the samples based on Al_2O_3 and P_2O_5/Al_2O_3 is 225–260 m^2/g. The pore volume and average pore diameter of CTA oxide and the NMTs-3-I catalyst are substantially smaller than the corresponding parameters of Al_2O_3 and HMA-4-I (Table 5). The supporting of the active component leads to a decrease in S_{sp}, V_{por}, and d_{av} relative to the corresponding parameters of the support (Table 5). It can be assumed that the active component on alumina prepared by precipitation has a higher degree of dispersion.

The active component distribution on the support surface can be judged from IR spectroscopic data. The supporting of the Ni–Mo-containing compound on phosphorus-promoted aluminum oxides is accompanied by the disappearance of the absorption bands of all hydroxyl groups (Fig. 3), indicating the uniform coverage of the surface with the precursor of the active component, regardless of the alumina nature. The spectra of CO adsorbed on the Ni–Mo–O/P_2O_5/CTA oxide and Ni–Mo–O/P_2O_5/Al_2O_3-1 samples pumped at 500°C exhibit only absorption bands assignable to CO complexes with molybdenum ions: Mo^{5+}–CO (2194 cm^{-1}), Mo^{4+}–$(CO)_2$ (2126, 2085 cm^{-1}), and Mo^0–CO (2040 cm^{-1}). The Mo^{6+} ion does not adsorb CO [35].

The catalytic properties of the Ni- and Co-containing samples on various supports were studied in the hydrodesulfurization of the diesel fraction at different process durations. As can be seen from the data in Table 4, the Ni-containing catalysts unpromoted with phosphorus have low activity, regardless of the support nature. The introduction of phosphorus enhances their efficiency, and the catalyst based on Al_2O_3-1 exhibits the highest activity. The lower the total concentration of terminal OH groups in the support (which decreases upon the introduction of phosphorus), the higher the activity of the Ni-containing catalyst (Tables 2, 4). As was demonstrated above, the concentration of terminal OH groups decreases in the following order:

$$Al_2O_3\text{-}1 > \text{CTA oxide}$$

$$> P_2O_5/\text{CTA oxide} > P_2O_5/Al_2O_3\text{-}1.$$

The residual sulfur content in the diesel fraction after its hydrodesulfurization on the Ni–Mo catalysts decreases in the same order:

Sample	Ni–Mo/Al_2O_3-1	Ni–Mo/CTA oxide	Ni–Mo/P/CTA oxide	Ni–Mo/P/Al_2O_3-1
S, ppm	1290	1136	333	178

Therefore, alumina, a support whose surface contains a smaller number of terminal OH groups, provides a higher catalytic activity. A decrease in the concentration of terminal OH groups is favored by the introduction of phosphorus, whose influence is especially pronounced for alumina prepared by precipitation. When phosphorus is introduced into Al_2O_3-1 and CTA oxide, the surface concentration of terminal OH groups decreases by a factor of 2.8 and 1.4, respectively, although the P/Mo ratio in the NMTs-3-I and NMA-4-I catalysts is the same (Table 4).

The cobalt catalysts are more active than the nickel catalysts. However, the active metal content of the cobalt catalysts is higher by a factor of ~1.5. An analysis of the data in Table 4 shows that the catalyst becomes more active when phosphorus is introduced simultaneously with the Mo-containing compound, not when phosphorus is supported earlier (compare the KMA-5-I and KMA-6-IIa samples). Perhaps this is due to the fact that the simultaneous introduction of the components affords phosphorus–molybdenum complexes [22, 36] facilitating the formation of the active

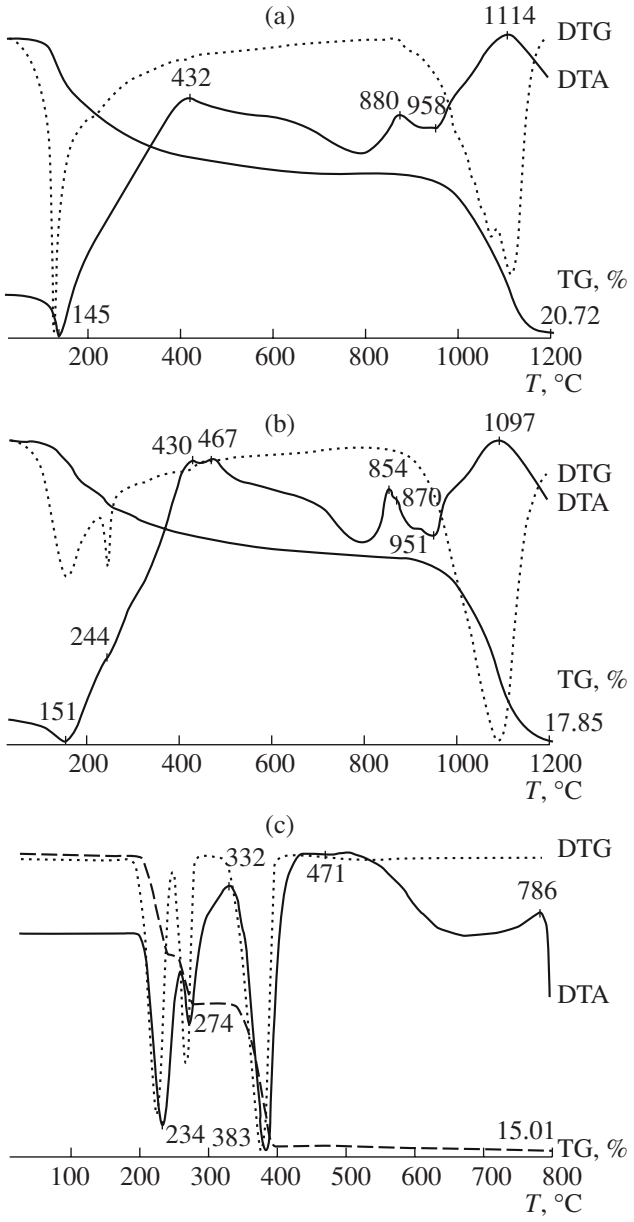

Fig. 1. TG curves of (a) Mo/Al_2O_3-1, (b) Mo/CTA oxide, and (c) ammonium paramolybdate.

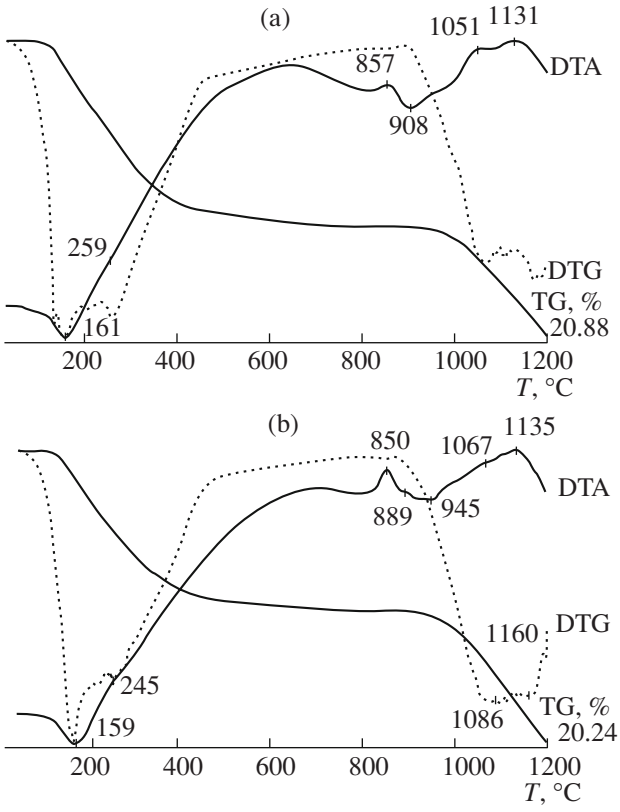

Fig. 2. TG curves of (a) Ni–$Mo/P_2O_5/Al_2O_3$-1 and (b) Ni–Mo/P_2O_5/CTA oxide.

oxide phase. For this reason, the subsequent samples were prepared by this method. An increase in the phosphorus content also enhances the catalytic activity (compare KMA-7-IIa and KMA-8-IIa). By optimizing the catalyst composition and heat treatment conditions, we obtained the most active Co-containing catalyst, for which the residual sulfur content of diesel fuel after purification was as low as 25 ppm (KMA-10-IIa). The replacement of citric acid with a solution of poly(ethylene oxide) did not enhance the catalytic activity.

X-ray diffraction and electron microscopic studies were carried out to reveal the nature of the active state of the KMA-10-IIa catalyst. The phase composition and local structure of the γ-Al_2O_3 support and Co–Mo catalyst before and after hydrodesulfurization were studied by the X-ray diffraction and EDRD methods. Fragments of the corresponding diffraction patterns are shown in Fig. 4. The diffraction patterns from the catalysts and support are very similar, but the intensity ratios of the reflections 3.1.1. ($2\theta \approx 16.4°$) and 2.2.2. ($2\theta \approx 17.3°$) are different, indicating changes in the cationic sublattice of the spinel structure of the support. The diffraction peaks 4.0.0. ($2\theta = 20.3°$) and 4.4.0. ($2\theta = 28.8°$) remain in their positions, which are determined by the dense packing of the oxygen ions.

Initial Catalyst

The diffraction pattern from the initial catalyst (before the reaction) has new diffraction peaks that are not observed for the support (Fig. 4). They can be assigned to the following crystalline phases: tetragonal MoO_2 ($2\theta = 11.7°$, 16.55°, 23.5°, and 28.8°; no. 99714 in the ICSD catalog; space group $P4_2/mnm$, a = 4.8473 Å, c = 2.8136 Å) and the monoclinic phases $Al_2(MoO_4)_3$ (2θ = 10.55°, 11.8°, 13.85°, and 14.25°; ICSD no. 202658; space group $P2_1/a$, a = 15.3803 Å, b = 9.0443 Å, c = 17.8880 Å, β = 125.382°) and $CoMoO_4$ (ICSD no. 281235, space group $P2/c$, a = 4.6598 Å, b = 5.6862 Å, c = 4.9159 Å, β = 90.521°).

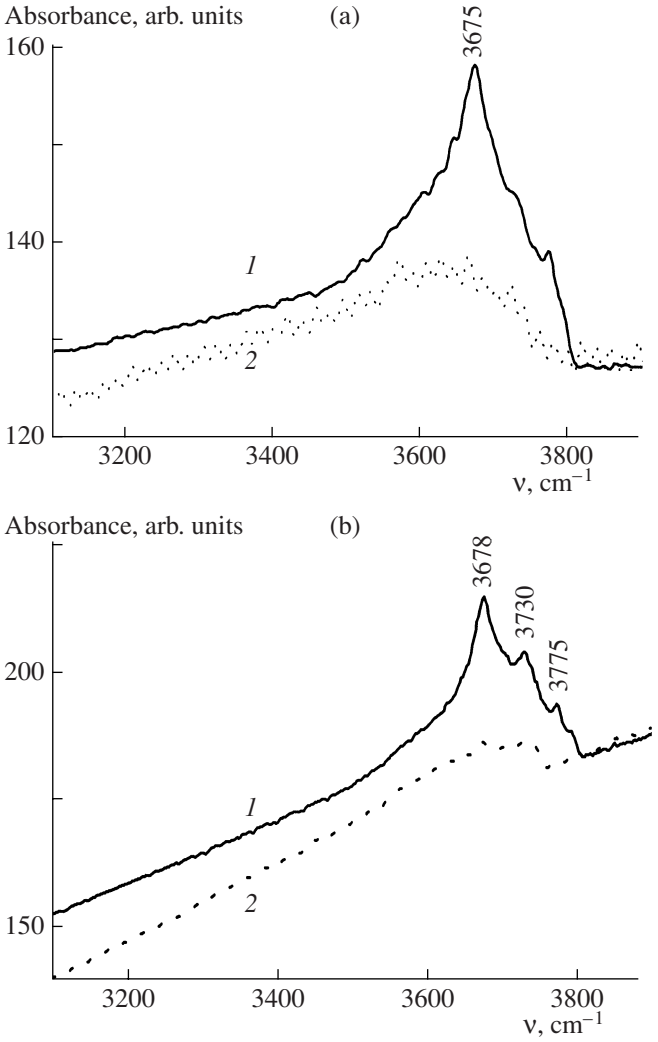

Fig. 3. IR spectra of the hydroxyl groups in the phosphorus-promoted (a) CTA oxide and (b) Al_2O_3 samples after pumping at 500°C: (*1*) before and (*2*) after Ni–Mo compound supporting.

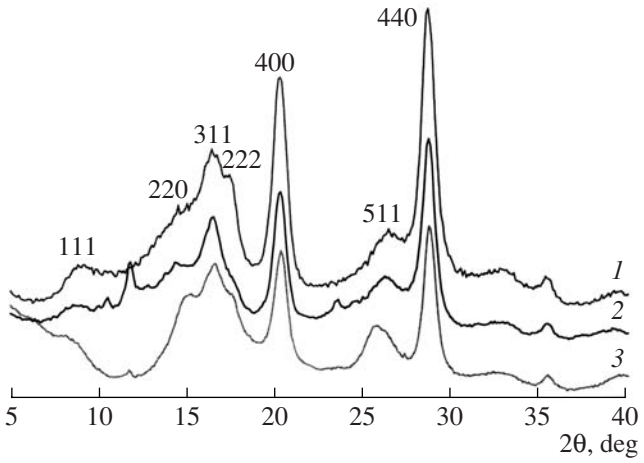

Fig. 4. Fragments of the diffraction patterns from (*1*) the support and (*2*, *3*) the KMA-10-IIa catalyst (*2*) before and (*3*) after the reaction.

This is seen well from a comparison between the IDC for the initial catalyst and the model diffraction patterns of these phases (Fig. 5). Note that the proportion of these phases is small.

An analysis of the EDRD curves shows that the local structure of the catalyst repeats the support structure, but the amplitude of the coordination peaks is increased possibly due to the incorporation of molybdenum ions into the spinel structure of the support. In order to observe the finely dispersed phases of molybdenum oxides, which do not show themselves in the diffraction patterns from the catalyst because of the significant broadening of the diffraction peaks, we constructed the difference EDRD curve and compared it with the model EDRD curves for the molybdenum oxides, namely, tetragonal MoO_2 and orthorhombic MoO_3 (ICSD no. 35076, space group *Pbnm*, a = 3.9628 Å, b = 13.8550 Å, c = 3.6964 Å). It turned out that molybdenum oxides of this composition are not the main phases of the initial catalyst. A comparison of the EDRD curves for the initial catalyst (derived from the IDC) and the model curves for monoclinic $Al_2(MoO_4)_3$, $CoMoO_4$, and cubic $CoAl_2O_4$ (ICSD no. 78403, space group $Fd\bar{3}m$, a = 8.1056 Å) shows (Fig. 6) that these compounds can be components of the catalyst. It is not impossible that all components interact when the Mo- and Co-containing components are supported.

Catalyst after the Reaction

Fragments of the diffraction patterns from the support, the IDC for the catalyst after the reaction, and the model EDRD curve for the MoS_2 structure (space group $P6_3/mmc$, a = 3.1602 Å, c = 12.294 Å) are shown in Fig. 7. The 00l and h0l peaks are very diffuse, although they are the strongest for the MoS_2 structure. The broadening of peaks of this type for layered structures, in which the parameter a is considerably smaller than the parameter c, is due to the disordered stacking of the layers. In the case considered, complete disordering and even the formation of a two-dimensional phase (MoS_2 as a single structural package) in place of the three-dimensional phase are possible. In order to consider this phenomenon in greater detail, the complete model EDRD curve was represented as two partial curves, one corresponding to the interatomic distances in the compact package of the MoS_2 structure and the other corresponding to the interpackage spacings. The difference curve for the catalyst and, for comparison, two model curves are shown in Fig. 8. Almost no interpackage spacings are observed in the layered MoS_2 structure. To see whether the Co cations are in the MoS_2 structure or not, the EDRD curve for the structure of the layer was presented as partial curves corresponding to the Mo–Mo, Mo–S, and S–S interatomic distances. The

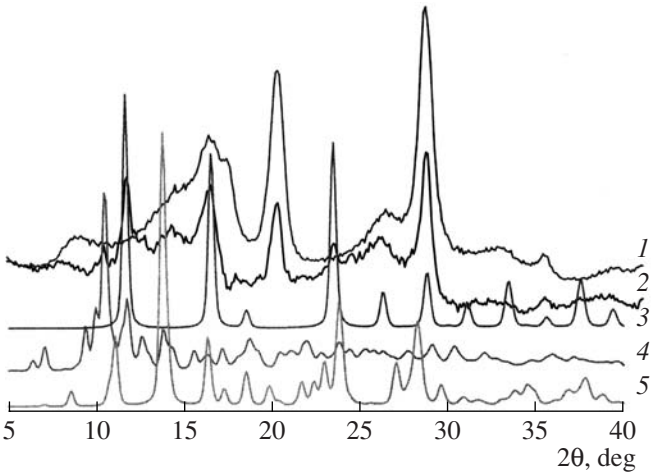

Fig. 5. Comparison of the intensity difference curves for (*2*) the initial KMA-10–IIa catalyst with the model diffraction patterns of the (*3*) MoO_3, (*4*) $Al_2(MoO_4)_3$, and (*5*) $CoMoO_4$ phases and with (*1*) the diffraction pattern of the support.

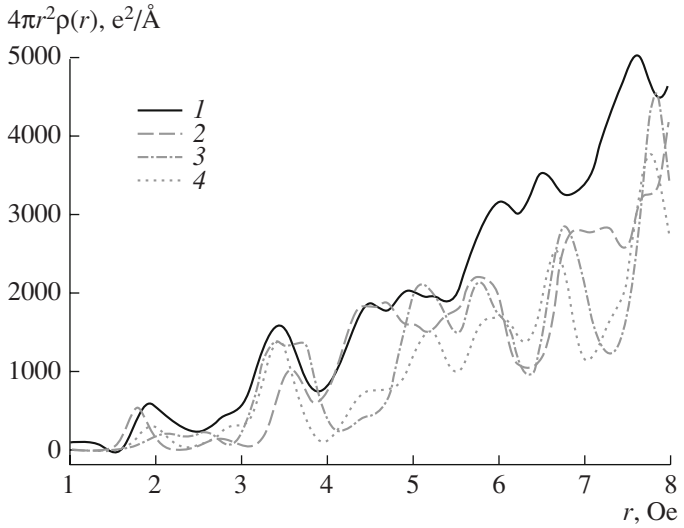

Fig. 6. (*1*) Electron density radial distribution curve of the initial KMA-10-IIa catalyst constructed on the basis of the IDC and the model EDRD curves for (*2*) monoclinic $Al_2(MoO_4)_3$, (*3*) $CoMoO_4$, and (*4*) $CoAl_2O_4$.

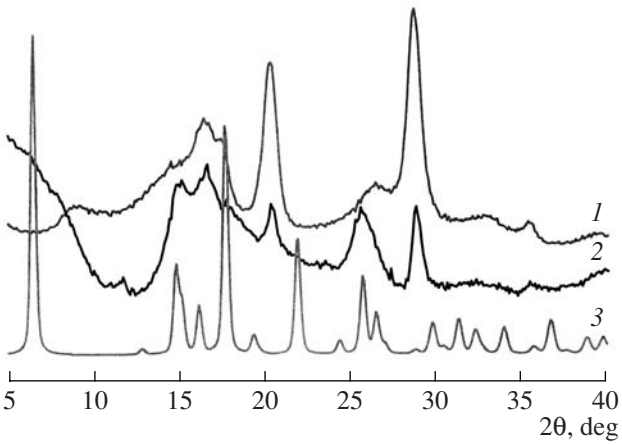

Fig. 7. (*1*) Fragment of the diffraction pattern from the support, (*2*) the DIC for the KMA-10-IIa catalyst after the reaction, and (*3*) the model EDRD curve for the MoS_2 structure.

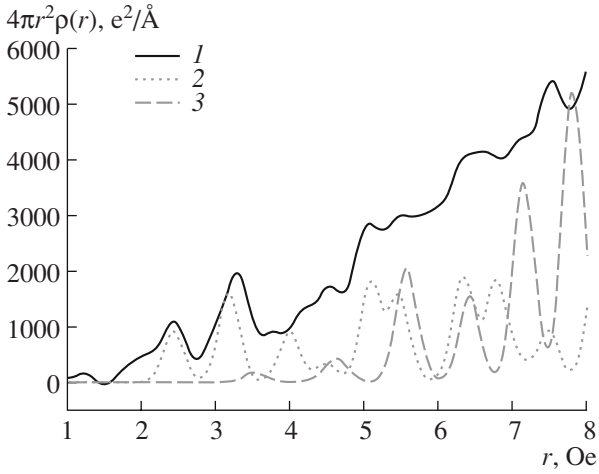

Fig. 8. (*1*) Difference curve for the KMA-10-IIa catalyst after the reaction versus two model curves including (*2*) interatomic distances inside the layer and (*3*) interatomic distances between layers.

shift of the metal–metal distances is probably caused by the incorporation of cobalt cations into the MoS_2 structure (inset in Fig. 9). An analysis of the data in Fig. 9, where the difference EDRD curve for the KMA-10-IIa sample after the reaction is compared to the model EDRD curves for the support structures, the MoS_2 layer, and $CoMo_2S_4$, shows that the cobalt ions can incorporate into the $CoMo_2S_4$ structure. Thus, the sulfidation of the sample and the hydrodesulfurization of the diesel fraction result in the transformation of the active component of the initial catalyst, which consists of a complicated Co–Mo–Al–oxide composition, into molybdenum sulfide doped with cobalt, and the latter, as a two-dimensional package, covers the support surface.

The images obtained by transmission electron microscopy (TEM) show that the initial KMA-10-IIa catalyst consists of porous crystalline aggregates 100 nm and more in size, including primary needlelike blocks 5–10 nm in diameter and 20–50 nm in length; the particles of the active Co–Mo component are dispersed on their surface (Fig. 10). The energy dispersive X-ray (EDX) spectra of different surface regions (I, II, etc.) indicate (Table 6) that large Co–Mo particles located in Al_2O_3 pores have different compositions: the Co content varies from ~5 at % (region III) to the value

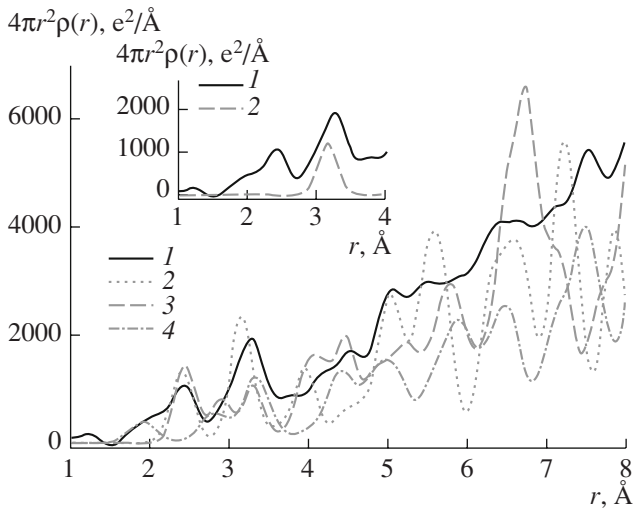

Fig. 9. Comparison between (*1*) the difference EDRD curve for the KMA-10-IIa sample after the reaction and the model EDRD curves for the (*2*) MoS_2 layer, (*3*) $CoMo_2S_4$ structure, and (*4*) γ-Al_2O_3 support. (*1*) The difference EDRD curve for the KMA-10 catalyst after the reaction and (*2*) the partial EDRD curve corresponding to the Mo–Mo interatomic distances inside the layer are shown in the inset.

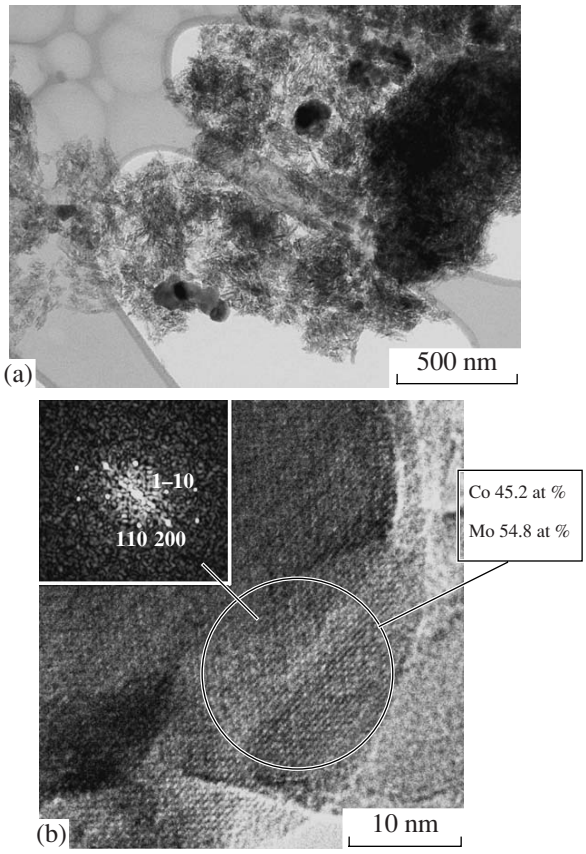

Fig. 10. (a) TEM and (b) HREM images of the surface of the initial KMA-10-IIa catalyst.

corresponding to Co/Mo ≈ 1 : 1 (region II), which is characteristic of the $CoMoO_4$ phase (Fig. 10). The composition of the fine fraction (Co–Mo clusters smaller than 1 nm in size) is the same throughout the initial catalyst, and the Co/Mo ratio is near 1 : 2 (Table 6).

After the reaction, the catalyst surface contains single-layer particles and multilayer aggregates (Fig. 11a) and large particles are also encountered (Fig. 11b). As in the initial catalyst, the Co, Mo, and S contents of large Co–Mo–S particles vary (Table 6). The particles have a smaller amount of sulfur than is necessary for the formation of bulk MoS_2. Therefore, the "sulfurization" of the large particles does not occur uniformly throughout the particle volume, but only at the surface, as can be seen in the TEM images (Fig. 11b). The layered MoS_2 structure is formed only in the subsurface layer. The compositions of the two-dimensional sulfide association species (2*d* clusters) are the same, and the Co/Mo ratio in the surface clusters is approximately the same as that in the initial sample (Table 6). The sulfur content of the dispersed association species is lower than is implied by the MoS_2 stoichiometry. This is likely due to the fact that the surface is dominated by single-layer association species and sulfur at the boundary with the alumina phase can be replaced by oxygen.

Table 6. Elemental composition of the catalyst before and after hydrodesulfurization (according to the energy dispersive X-ray analysis)

Element	Element content, at %					
	large Co–Mo particles				Co–Mo clusters	
	I	II	III	IV	I	II
	Initial catalyst					
Co	45.2	47.3	4.7	8.1	37.5	31.5
Mo	54.8	52.7	95.3	91.9	62.5	68.5
	Catalyst after reaction					
S	22.9	36.7	–	–	51.6	50.6
Co	5.2	11.4	–	–	19.4	19.6
Mo	71.9	51.9	–	–	29.1	29.7

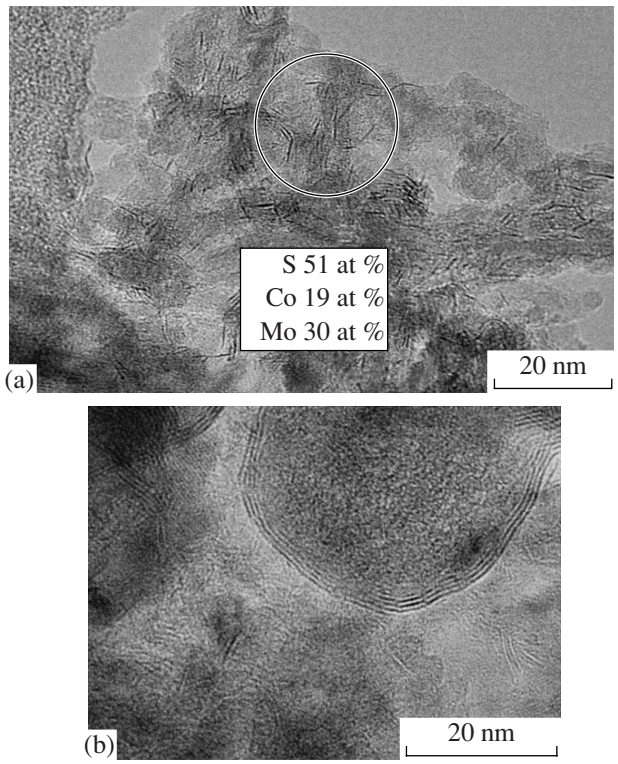

Fig. 11. Electron micrographs of the KMA-10-IIa catalyst after the reaction: (a) clusters and (b) large particles.

The association species are layered, and the interlayer spacing is 0.62–0.67 nm, which is close to the parameter d_{002} = 0.615 nm of hexagonal molybdenite (MoS_2). Therefore, the presence of other sulfide phases (such as Mo_2S_3, Mo_3S_4, and others) can be excluded. The Co ions can be components of the Co–Mo–S association species. In the single-layer association species, they can be located both at the edges of the disulfide MoS_2 packages and on basal planes. If the association species consist of two MoS_2 layers or more, cobalt can also be intercalated into the interlayer spaces of the structure. In this case, the formation of particles of the monoclinic $CoMo_2S_4$ phase [37] with the lattice parameters a = 11.8 Å, b = 6.6 Å, c = 12.7 Å, and $\beta = 90°$ cannot be excluded. This phase is also layered, with an interlayer spacing of c = 0.575 nm and a hexagonal motif of the S and Mo atomic packing in the *XY* plane. In this structure, the Co ions are intercalated into the interlayer spacings of the MoS_2 packages and are in an octahedral environment of sulfur ions. This phase should possess [11] an enhanced activity in fuel hydrodesulfurization. Note that, according to EDX data, the average elemental composition of the dispersed Co–Mo–S association species corresponds to the formula $Co_2Mo_3S_5$ ($Co_{1.3}Mo_2S_{3.3}$), which is distinct from the stoichiometry of the bulk $CoMo_2S_4$ phase. This difference is explained by the small size of the association species: in this case, some sulfur ions can be replaced by oxygen ions linking the MoS_2 packages to the Al_2O_3 support. At the same time, the presence of excess Co atoms (over the Co content of $CoMo_2S_4$) can be explained by the location of some amount of cobalt at the lateral edges of both multilayer and single-layer MoS_2 packages. Thus, taking into account the replacement of some sulfur ions by the oxygen ions and the location of part of Co at the package edges, we can assume that the composition of the Co–Mo–S association species is quantitatively formed as follows: $Co_{0.3}$ are the atoms at the association species edges, $Co_{1.0}$ are the atoms intercalated into $Mo_2S_{3.3}$, and the missing $S_{0.7}$ atoms are replaced by an equal amount of oxygen at the boundary with the Al_2O_3 phase.

Therefore, to achieve the active state of the catalyst, it is necessary, first of all, that cobalt fill the interlayer space in the association species through intercalation. It is also necessary that cobalt be fixed at the association species edges to form the most active hydrodesulfurization sites containing weakly bound Co. This is a possible explanation of the fact that the catalyst with the optimum atomic ratio of Co/Mo = 0.66 is the most active.

REFERENCES

1. Nefedov, B.K., *Katal. Prom–sti.*, 2003, no. 2, p. 20.
2. Song, C., *Catal. Today*, 2003, vol. 86, p. 211.
3. Gates, B.C. and Topsøe, H., *Polyhedron*, 1997, vol. 16, p. 3213.
4. Topsøe, H, Clausen, B.S, and Massoth, F.E, in *Catalysis—Science and Technology*, Anderson, J.R. and Boudard, M., Eds., Berlin: Springer, 1996, vol. 11.
5. Topsøe, H. and Clausen, B.S., *Catal. Rev. Sci. Eng.*, 1984, vol. 26, p. 395.
6. Topsøe, H., Clausen, B.S., Topsøe, N., and Pederson, E., *Ind. Eng. Chem. Fundam.*, 1986, vol. 25, p. 25.
7. Clausen, B.S., Mørup, S., Topsøe, H., and Candia, R., *J. Phys. Colloq.*, 1976, vol. 37.
8. Topsøe, H., Clausen, B.S., Candia, R., Wivel, C., and Mørup S, *J. Catal.*, 1981, vol. 68, p. 433.
9. Wivel, C., Candia, R., Clausen, B.S., Mørup, S., and Topsøe, H., *J. Catal.*, 1982, vol. 68, p. 453.
10. Topsøe, H., Clausen, B.S., Candia, R., Wivel, C., and Mørup, S., *Bull. Soc. Chim. Belg.*, 1981, vol. 90, p. 1189.
11. Bouwens, S.M.A.M., van Zon, F.B.M., van Dijik, M.P., van der Kraan, A.M., de Beer, V.H.J., van Veen, J.A.R., and Koningsberger, D.C., *J. Catal.*, 1994, vol. 146, p. 375.
12. Luck, F., *Bull. Soc. Chim. Belg.*, 1991, vol. 100, p. 781.
13. Breysse, M., Portefaix, J.L., and Vrinat, M., *Catal. Today*, 1991, vol. 10, p. 489.
14. RF Patent 2313390, 2007.
15. Kul'ko, E.V., Ivanova, A.S., Kruglyakov, V.Yu., Moroz, E.M., Shefer, K.I., Litvak, G.S., Kryukova, G.N., Tanashev, Yu.Yu., and Parmon, V.N., *Kinet. Katal.*, 2007, vol. 48, no. 2, p. 332 [*Kinet. Catal.* (Engl. Transl.), vol. 48, no. 2, p. 316].
16. Price, W., *Analytical Atomic Absorption Spectroscopy*, New York: Wiley-Interscience, 1972.

17. Umanskii, Ya.S., *Rentgenografiya metallov* (X-ray Diffraction Characterization of Metals), Moscow: Metallurgiya, 1970.
18. Moroz, E.M., *Usp. Khim.*, 1992, vol. 61, p. 356.
19. Moroz, E.M., Zyuzin, D.A., Shefer, K.I., and Isupova, L.A., *Zh. Strukt. Khim.*, 2007, vol. 48, p. 753 [*J. Struct. Chem.* (Engl. Transl.), vol. 48, p. 704].
20. Buyanova, N.E., Karnaukhov, A.P., and Alabuzhev, Yu.A., *Opredelenie poverkhnosti dispersnykh i poristykh materialov* (Determination of the Specific Surface Area of Disperse and Porous Materials), Novosibirsk: Inst. Kataliza, 1978.
21. Paukshtis, E.A., *Infrakrasnaya spektroskopiya v geterogennom kislotno-osnovnom katalize* (Infrared Spectroscopy in Heterogeneous Acid–Base Catalysis), Novosibirsk: Nauka, 1992.
22. Atanasova, P., Halachev, T., Uchytil, J., and Kraus, M., *Appl. Catal.*, 1988, vol. 38, p. 235.
23. Matralis, H.K., Lycourghiots, A., Grange, P., and Delmon, B., *Appl. Catal.*, 1988, vol. 38, p. 273.
24. Kwak, C., Kim, M.Y., Choi, K., and Moon, S.H., *Appl. Catal., A*, 1999, vol. 185, p. 19.
25. Kwak, C., Lee, J.J., Bae, J., Choi, K., and Moon, S.H., *Appl. Catal., A*, 2000, vol. 200, p. 233.
26. Moon, S.H., *Catal. Surv. Asia*, 2003, vol. 7, p. 11.
27. Mangnus, P.J., van Veen, J.A.R., Eijsbouts, S., de Beer, V.H.J., and Moulijn, J.A., *Appl. Catal.*, 1990, vol. 61, p. 99.
28. Mangnus, P.J., van Langeveld, A.D., de Beer, V.H.J., and Moulijn, J.A., *Appl. Catal.*, 1991, vol. 68, p. 161.
29. Okamoto, Y., Ochiai, K., Kawano, M., Kobayashi, K., and Kubota, T., *Appl. Catal., A*, 2002, vol. 226, p. 115.
30. Borque, M.P., Lopez-Agudo, A., Olguin, E., Vrinat, M., Cedeno, L., and Ramirez, J., *Appl. Catal., A*, 1999, vol. 180, p. 53.
31. Massoth, F.E., *Adv. Catal.*, 1978, vol. 27, p. 265.
32. Okamoto, Y. and Imanaka, T., *J. Phys. Chem.*, 1988, vol. 92, p. 7102.
33. Ivanova, A.S., Litvak, G.S., Kryukova, G.N., Tsybulya, S.V., and Paukshtis, E.A., *Kinet. Katal.*, 2000, vol. 41, no. 1, p. 137 [*Kinet. Catal.* (Engl. Transl.), vol. 41, no. 1, p. 122].
34. Li, H., Shen, B., Zhang, W., Zhao, Y., Wang, X., Zhang, Z., and Shen, S., *Fuel*, 2006, vol. 85, p. 2445.
35. Hadjiivanov, K.I. and Vayssilov, G.N., *Adv. Catal.*, 2002, vol. 47, p. 307.
36. Caceres, C.V., Fierro, J.L.G., Blanco, M.N., and Thomas, H.J., *Appl. Catal.*, 1984, vol. 10, p. 333.
37. Vaqueiro, P., Kosidowski, M.L., and Powell, A.V., *Chem. Mater.*, 2002, vol. 14, no. 3, p. 1201.